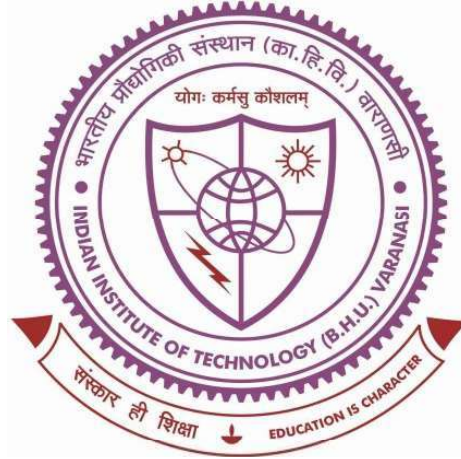


DEVELOPMENT OF BINARY, TERNARY, AND HIGH ENTROPY Ti ALLOYS FOR BIOMEDICAL IMPLANT APPLICATIONS



Thesis submitted in partial fulfillment for the
Award of Degree

Doctor of Philosophy

By

Rupesh Kumar

DEPARTMENT OF MECHANICAL ENGINEERING
INDIAN INSTITUTE OF TECHNOLOGY
(BANARAS HINDU UNIVERSITY)
VARANASI - 221005

Roll No. 19131502

2024

RECOMMENDATION

This chapter summarizes the key conclusions drawn from the investigation of various Ti alloys developed via conventional sintering. It also outlines the potential directions for future research aimed at improving the understanding and performance of these materials within the scope of the present study.

7.1 Conclusions

This study successfully developed and characterized binary, ternary, and high-entropy Ti-based alloys tailored for load-bearing biomedical implant applications. The main conclusions drawn from the experimental results and analyses are as follows:

Phase composition

- XRD analysis of binary Ti-xNb and Ti-xZr, and Ti-10Zr-xNb powders shows individual elemental peaks with no evidence of oxidation or intermetallic compounds, indicating effective milling under controlled inert atmosphere and use of toluene.
- For $\text{TiNb}_{1.5}\text{Mo}_{0.1}\text{Zr}_{1.15}\text{Cu}_{0.25}$ powders, peak broadening and gradual disappearance of minor elemental peaks (Ti, Cu, Zr) occur with increased milling time, indicating solid solution formation and lattice strain. After prolonged milling, the powder consists mainly of two BCC phases (BCC1 and BCC2) with some undissolved Zr, showing a complex multiphase structure.
- For $\text{TiNbZr}_{0.8}\text{Mo}_{0.92}\text{Sn}_{0.28}$ powders, initial disappearance of Sn and minor Mo peaks is observed with milling time. After extended milling, the powder exhibits three phases: BCC1, BCC2, and HCP, demonstrating progressive solid solution formation and phase evolution typical of complex alloying with residual HCP phase from Zr.

- Commercial cpTi shows single α -phase (HCP) structure, while Ti-6Al-4V exhibits a dual-phase microstructure with α (HCP) and β (BCC) phases due to Al and V alloying effects.
- Sintered Ti-xNb alloys contain both α and β phases, with β phase fraction increasing as Nb content increases, demonstrating Nb's role in stabilizing the β phase.
- Sintered Ti-xZr alloys retain a single α -phase with peak shifts towards lower angles caused by lattice parameter increase from Zr substitution.
- Sintered Ti-10Zr-xNb alloys contain mixed α and β phases, with peak shifts indicating Nb incorporation and β phase stabilization; no intermetallic or secondary phases are detected.
- For TiNb_{1.5}Mo_{1.1}Zr_{1.15}Cu_{0.25}, the sintered alloy shows a predominant BCC1 phase along with tetragonal and orthorhombic phases.
- For TiNbZr_{0.8}Mo_{0.92}Sn_{0.28}, the sintered alloy exhibits BCC1, BCC2, and orthorhombic phases.

Microstructural Analysis

- The microstructure of cpTi consists of a single-phase α -Ti with equiaxed grains, while Ti-6Al-4V exhibits a biphasic microstructure of primary α -phase and intergranular β -phase.
- In sintered Ti-Nb binary alloys, the addition of Nb induces a duplex microstructure with α -phase and β -phase, where Nb stabilizes the β -phase. Needle-like dendritic structures form and increase with Nb content, with elemental mapping confirming uniform Nb distribution enriched in β -phase regions.

- Sintered Ti-Zr binary alloys show two α -phase distributions: one Ti-rich and one Zr-rich, both with hexagonal close-packed structure. Increasing Zr content leads to coarser grains and more Zr-rich α -phase, with homogeneous Zr distribution confirming solid solution formation without phase segregation.
- Ternary Ti-10Zr-xNb alloys exhibit duplex microstructure with α -Ti with hexagonal close-packed and β -Ti with BCC phases. Nb addition suppresses β -to- α transformation, stabilizing the β phase.
- Sintered high entropy alloys $\text{TiNb}_{1.5}\text{Mo}_{0.1}\text{Zr}_{1.15}\text{Cu}_{0.25}$ and $\text{TiNbZr}_{0.8}\text{Mo}_{0.92}\text{Sn}_{0.28}$ exhibit complex multiphase microstructures with dominant BCC1 phase, and secondary tetragonal, orthorhombic, and BCC2 phases, with elemental mapping shows homogeneous distribution of all constituent elements, indicating stable solid solutions.

Density and Porosity

- Theoretical densities of cpTi and Ti-6Al-4V were used as benchmarks; no porosity data were recorded for them as they were not produced via powder metallurgy.
- Ti-Nb binary alloys showed increasing density with Nb addition, ranging from 4.096 to 4.346 g/cm³, accompanied by 11-15% porosity, reflecting the influence of Nb's higher atomic mass and reduced diffusion kinetics during sintering.
- Ti-Zr binary alloys exhibited densities between 4.609 and 4.885 g/cm³ with a relatively stable ~9% porosity, suggesting uniform sintering and limited influence of Zr on densification resistance.
- Ti-10Zr-xNb ternary alloys showed the lowest densities, ranging from 3.476 to 3.866 g/cm³, along with the highest porosities of 25-27%, indicating poor

densification likely due to phase mismatch and hindered sintering kinetics from combined Zr and Nb additions.

- Among high-entropy alloys, $\text{TiNb}_{1.5}\text{Mo}_{1.1}\text{Zr}_{1.15}\text{Cu}_{0.25}$ exhibited a density of 6.63 g/cm^3 with 9% porosity, whereas $\text{TiNbZr}_{0.8}\text{Mo}_{0.92}\text{Sn}_{0.28}$ had a slightly lower density of 6.41 g/cm^3 but a significantly higher porosity of 14%, suggesting compositional effects on sintering efficiency and packing behaviour.

Hardness and Elastic modulus

- cpTi exhibits a hardness of $178 \pm 4.35 \text{ HV}$ and an elastic modulus of $117.53 \pm 8.13 \text{ GPa}$, while Ti-6Al-4V shows higher hardness of $350 \pm 6 \text{ HV}$ and a slightly increased elastic modulus of $125 \pm 4.35 \text{ GPa}$ due to its $\alpha + \beta$ phase structure.
- Hardness in Ti-Nb alloys peaks at $403 \pm 21 \text{ HV}$ for Ti-10Nb due to solid solution strengthening and $\alpha + \beta$ phases, then decreases with higher Nb content with values of $359 \pm 20 \text{ HV}$ for Ti-15Nb and $292 \pm 23 \text{ HV}$ for Ti-20Nb as β phase dominates. Elastic modulus decreases with increasing Nb, reaching lowest of $43.5 \pm 4.9 \text{ GPa}$ for Ti-20Nb due to β phase stabilization. At 25 wt.% Nb, hardness increases again to $397 \pm 13 \text{ HV}$ with a slight rise in modulus to $50.9 \pm 3.3 \text{ GPa}$ attributed to ω phase formation.
- Hardness of Ti-Zr alloys increases with Zr addition up to 10 wt.% Zr, reaching highest of $539 \pm 27 \text{ HV}$ for Ti-10Zr, then slightly decreases at higher Zr levels such as $529 \pm 24 \text{ HV}$ for Ti-15Zr and $489 \pm 40 \text{ HV}$ for Ti-20Zr. Elastic modulus shows a similar trend, rising from 87.5 GPa for Ti-5Zr to 94.1 GPa for Ti-10Zr, then decreasing at higher Zr content with Ti-25Zr dropping to 71.5 GPa .
- In Ti-10Zr-xNb ternary alloys, hardness is highest at 5 wt.% Nb around 380 HV and remains relatively high at 10 wt.% Nb near 340 HV , then decreased significantly at 15 wt.% Nb showing the lowest hardness before increasing

again at 20 wt.% Nb. The elastic modulus decreases with increasing Nb content from 41.5 GPa at 5 wt.% Nb to 30.4 GPa at 15 wt.% Nb and then slightly rises to 32.5 GPa at 20 wt.% Nb.

- Hardness values are high for both HEAs: 470 ± 22 HV for $\text{TiNb}_{1.5}\text{Mo}_{1.1}\text{Zr}_{1.15}\text{Cu}_{0.25}$ and 481 ± 38 HV for $\text{TiNbZr}_{0.8}\text{Mo}_{0.92}\text{Sn}_{0.28}$. Elastic modulus is lower than cpTi, and are 69.1 GPa and 64.6 GPa, respectively, influenced by porosity (9.27% and 14.59%) and solid solution strengthening.

Electrochemical corrosion behaviour

- cpTi exhibits superior corrosion resistance with a lower corrosion rate of 0.0063 mm/year compared to Ti-6Al-4V, which shows a higher corrosion rate of 0.0126 mm/year, due to more stable passive oxide layer of cpTi, higher charge transfer resistance, and lower current density.
- Corrosion resistance decreased with increasing Nb content. Ti-5Nb exhibited the highest resistance with corrosion rate of 0.0075 mm/year, while Ti-20Nb showed the worst performance with corrosion rate of 0.0829 mm/year.
- Corrosion resistance improved with increasing Zr content. Ti-20Zr showed the best corrosion behaviour with the lowest corrosion rate of 0.00129 mm/year, along with the highest R_2 value of $1.35 \times 10^6 \Omega \cdot \text{cm}^2$.
- Corrosion resistance decreased with increasing Nb content. Ti-10Zr-5Nb exhibited the highest resistance with corrosion rate of 0.207 mm/year, while Ti-10Zr-20Nb showed the poorest performance with corrosion rate of 1.093 mm/year. EIS results confirmed higher R_2 ($2.35 \text{ k}\Omega \cdot \text{cm}^2$) for Ti-10Zr-5Nb alloy.
- Corrosion resistance was higher for $\text{TiNbZr}_{0.8}\text{Mo}_{0.92}\text{Sn}_{0.28}$ compared to $\text{TiNb}_{1.5}\text{Mo}_{1.1}\text{Zr}_{1.15}\text{Cu}_{0.25}$ HEA Sn exhibited a more positive E_{corr} (-0.3787 V) and lower I_{corr} ($2.71 \mu\text{A}/\text{cm}^2$), indicating better corrosion resistance and a more

stable passive film. In contrast, HEA Cu showed a more negative E_{corr} (-0.8145 V) and higher I_{corr} ($5.28 \mu\text{A}/\text{cm}^2$), reflecting poorer corrosion performance. EIS results confirmed a higher R_2 ($3.99 \text{ k}\Omega\cdot\text{cm}^2$) for HEA Sn compared to $3.66 \text{ k}\Omega\cdot\text{cm}^2$ for HEA Cu.

- The corrosion mechanism in these alloys primarily involves the formation and stability of passive oxide layers such as TiO_2 , Nb_2O_5 , and ZrO_2 , which protect the surface by limiting further electrochemical reactions; however, increased porosity and the presence of less stable or defective oxide films especially in Ti-10Zr-xNb and Cu-containing HEAs facilitate localized corrosion and accelerate degradation.

Tribological behaviour

- The cpTi exhibits a fluctuating friction coefficient at lower loads that stabilizes with increasing load, while Ti-6Al-4V maintains a more stable friction response overall. In terms of wear, cpTi shows wear volume increasing from 0.103 mm^3 to 0.606 mm^3 between 10 N and 40 N loads, whereas Ti-6Al-4V demonstrates better wear resistance with wear volume rising from 0.152 mm^3 to 0.541 mm^3 over the same range, indicating lower material loss under higher loads.
- Among the Ti-Nb sintered alloys tested under SBF conditions, Ti-10Nb exhibits the best wear resistance, showing the lowest wear volume of 0.038 mm^3 at 10 N, and increasing with the normal load. Alloys with Nb content above 10% show a slight increase in wear volume and rate but maintain favourable antiwear performance overall. This indicates that Nb addition significantly enhances wear resistance in Ti-Nb alloys, with 10% Nb providing optimal tribological performance.

- Among the Ti-Zr sintered alloys, increasing Zr content generally reduces wear volume, except for Ti-10Zr, which shows the highest wear volume of 0.3439 mm³ at 40 N and wear rate despite its high hardness. The Ti-15Zr alloy exhibits the lowest wear volume of 0.0044 mm³ at 10 N among the series, with wear volume increasing as the normal load increases.
- The ternary Ti-10Zr-xNb alloys exhibit higher friction coefficients compared to binary alloys, primarily due to increased porosity which enhances asperity interlocking. Friction generally increases with Nb content and load for lower Nb levels (5-10%), while higher Nb content (15-20%) shows a slight friction reduction at higher loads, likely due to wear debris acting as a lubricating intermediate layer.
- Ternary Ti-10Zr-xNb alloys show an optimal wear resistance at 15% Nb, with the lowest wear volumes of 0.04 mm³ at 20 N, 0.05 mm³ at 30 N, and 0.15 mm³ at 40 N. Wear volumes increase for both lower and higher Nb contents, e.g., Ti-10Zr-10Nb exhibits wear volumes as high as 0.32 mm³ (20 N), 0.76 mm³ (30 N), and 0.28 mm³ (40 N).
- The COF of the sintered HEAs increases slightly with load, with TiNb_{1.5}Mo_{0.1}Zr_{1.15}Cu_{0.25} exhibiting higher COF values (0.473 at 20 N and 0.490 at 30 N) compared to TiNbZr_{0.8}Mo_{0.92}Sn_{0.28} (0.368 at 20 N and 0.387 at 30 N).
- Wear volume and wear rate increase with load for both HEAs, with TiNb_{1.5}Mo_{0.1}Zr_{1.15}Cu_{0.25} showing greater wear (0.0061 mm³ at 20 N and 0.0361 mm³ at 30 N) than TiNbZr_{0.8}Mo_{0.92}Sn_{0.28} (0.0040 mm³ at 20 N and 0.0277 mm³ at 30 N)
- The cpTi and Ti-6Al-4V primarily exhibit adhesive and abrasive wear due to their relatively lower hardness; binary Ti-xNb and Ti-xZr alloys show mixed

abrasive and adhesive wear concentrated around pores and pits; ternary Ti-10Zr-xNb alloys mainly undergo adhesive wear linked to their softer surfaces; while the hardest high entropy alloys predominantly experience oxidative wear with minimal abrasive or adhesive damage.

Tribocorrosion behaviour

- The tribocorrosion study confirms that Ti-6Al-4V outperforms cpTi in both wear and electrochemical resistance under OCP and PDP conditions. Ti-6Al-4V showed lower wear volumes (0.289 mm^3 under OCP and 0.341 mm^3 under PDP) compared to cpTi (0.364 mm^3 under OCP and 0.491 mm^3 under PDP). This improved performance is attributed to Al and V in Ti-6Al-4V, which enhance passive film stability and reduce anodic dissolution and friction.
- The tribocorrosion analysis indicates that Ti-10Nb exhibits the best performance among all Ti-Nb alloys, with the lowest wear volume under both OCP (0.1111 mm^3) and PDP (0.0526 mm^3) conditions. This improvement is attributed to Nb's strong affinity for oxygen, promoting the growth of a Nb-enriched passive layer under electrochemical polarization. Conversely, alloys with higher Nb content (Ti-20Nb, Ti-25Nb) showed increased wear volumes due to reduced hardness and less effective passivation under combined mechanical and electrochemical condition.
- Ti-15Zr demonstrated the highest tribocorrosion resistance among Ti-Zr compositions, with the lowest wear volume under both OCP (0.0124 mm^3) and PDP (0.0080 mm^3) conditions. Moderate Zr addition improves oxide layer stability and wear resistance, whereas excessive Zr content (e.g., Ti-25Zr) leads to increased wear volume (0.0863 mm^3 OCP; 0.0491 mm^3 PDP), likely due to microstructural changes and reduced electrochemical stability.

- The tribocorrosion analysis of ternary alloys reveals that Ti-10Zr-15Nb exhibits the best overall performance among the ternary alloys, with a significantly lower wear volume under PDP (0.088 mm³) and relatively low wear under OCP (0.193 mm³).
- The tribocorrosion analysis of TiNb_{1.5}Mo_{0.1}Zr_{1.15}Cu_{0.25} and TiNbZr_{0.8}Mo_{0.92}Sn_{0.28} confirms that wear resistance improves under PDP conditions due to enhanced passive film stability. HEA-Cu showed a significant reduction in wear volume from 0.0337 mm³ (OCP) to 0.0109 mm³ (PDP), while HEA-Sn exhibited a decrease from 0.0185 mm³ to 0.0142 mm³.

The findings revealed that appropriate alloying with Nb, Zr, Mo, Cu, and Sn enables tuning of the β -phase content, solid solution strengthening, and passive film stability, critical for achieving a desirable balance of low elastic modulus, high hardness, corrosion resistance, and excellent wear performance. In particular, Ti-10Nb, Ti-15Zr, Ti-10Zr-15Nb, and Sn-containing HEAs emerged as optimal compositions due to their superior mechanical integrity and electrochemical stability. These alloys demonstrate superior biomechanical compatibility through reduced elastic modulus, aligning more closely with natural bone and minimizing stress shielding. Enhanced resistance to corrosion, wear, and tribocorrosion, particularly in HEAs and select ternary compositions, contributes to improved long-term durability in physiological environments. Compared to commercial alloys like cpTi and Ti-6Al-4V, the newly developed materials offer a more favourable balance of mechanical and electrochemical performance. These alloys demonstrate superior biomechanical compatibility through reduced elastic modulus, aligning more closely with natural bone and minimizing stress shielding. Enhanced resistance to corrosion, wear, and tribocorrosion, particularly in HEAs and select ternary compositions, contributes to improved long-term durability in

physiological environments. Compared to commercial alloys like cpTi and Ti-6Al-4V, the newly developed materials offer a more favourable balance of mechanical and electrochemical performance.

7.2 Future scope

This study has provided an in-depth investigation into the phase formation, mechanical behavior, and electrochemical performance of novel Ti-based alloys, several areas remain open for further exploration to bridge the gap between lab-scale development and clinical translation:

- The in vitro biocompatibility and in vivo animal studies should be extended to understand the osseointegration and host tissue response to the developed Ti alloys under actual physiological conditions.
- The wear and corrosion studies should be conducted under pathological environments, such as acidic pH, inflammatory conditions, or oxidative stress, which better simulate the clinical failure environment of implants.
- The optimized alloys from this study may be processed via additive manufacturing techniques to fabricate porous implants with tailored architecture, enabling stress-shielding mitigation and enhanced bone ingrowth.
- Tribocorrosion-fatigue synergy should be studied in SBF environments to capture the realistic degradation behaviour under combined mechanical and electrochemical conditions.
- The alloys can be further functionalized by bioactive surface coatings (e.g., hydroxyapatite, Zn-doped TiO₂, Ag coatings) to improve bioactivity and antibacterial performance.

- Computational tools like CALPHAD and thermodynamic modelling should be employed to predict phase stability, assist in multi-component alloy design, and optimize processing routes for biomedical Ti alloys.